PHYSICAL REVIEW A VOLUME 32, NUMBER 5 NOVEMBER 1985

Multichannel quantum-defect theory and an equivalent N-level system

W. E. Cooke and C. L. Cromer*
Physics Department, University of Southern California, Los Angeles, California 90089-0484
(Received 11 March 1985)

A derivation and geometrical interpretation of multichannel quantum-defect theory (MQDT) is presented. An alternative set of MQDT parameters is suggested which separates into two independent groups, one representing the quantum defect of a Rydberg series in the absence of channel coupling and the other representing the channel coupling itself. An equivalent N-level system is developed so that the MQDT boundary conditions are replaced by a simple energy restriction on the N-level system, resulting in easier solutions of the equations. The equations are solved and spectra are presented for the simple two-channel case and for the three-channel case, where channel interactions lead to interferences in the spectra.

I. INTRODUCTION

Over the past decade, multichannel quantum-defect theory (MQDT) has been successfully used to characterize the complex bound-state spectra of many two-electron-like atoms. Originally formulated in 1966 by Seaton,[1] MQDT was not used extensively to characterize multielectron spectra until Fano and Lu developed a graphical analysis technique in 1970.[2] Since then, laser spectroscopy has dramatically increased the amount and accuracy of spectral data on two-electron Rydberg states, and the use of MQDT for its analysis has become much more common.[3–6]

In Fano's original work,[7] he discussed the problem of the photoabsorption spectrum of H_2, a case where the two initial electronic wave functions are in distinguishable molecular orbits. His formalism quite naturally made maximal use of the molecular (or close-coupled) symmetry of the initial state. However, for studies of the properties of Rydberg states—including their behavior in fields and their photoabsorption spectra—much can be gained by exploiting the difference between the Rydberg electron wave function and the other core electrons' wave functions. In this manuscript we will reformulate the MQDT equations to do this. In so doing, we will arrive at a formulation much closer to Seaton's original work,[1] although the development is closer in spirit to Fano's.

The Fano formalism basically satisfies the boundary conditions for a small radius r where one can take advantage of the close-coupled symmetry and integrates to large r where the other boundary conditions are applied. Here we will reverse the procedure by integrating from large r, where the Rydberg wave-function characteristics are simple, into small-r values and then applying the final boundary conditions. Initially, however, we will formulate the MQDT equations in a symmetric fashion which illustrates how either route may be pursued.

As a result of the reversal of the roles of large r and small r in developing MQDT, we will use a set of parameters that is related to, but different from, those that Fano defined. In particular, we will define a constant quantum defect to characterize a Rydberg series, even though no bound states of that series may have that value. In fact, the difference between a particular Rydberg state's quantum defect and the series value will simply determine the relative amount of configuration mixing in that state. Configuration mixing, or channel mixing in MQDT parlance, will be parametrized by two-electron interaction matrix elements calculated using single-configuration Rydberg states.

Our motivation for an MQDT analysis parametrized in such a fashion has originated from photoionization studies of Rydberg states using the isolated core excitation (ICE) technique[8] to excite autoionizing states. With this technique, autoionizing states are produced by exciting the inner electron of a bound, singly excited Rydberg state, as in the strontium transition $5snl \rightarrow 5pnl$. For this type of transition, the Rydberg electron's wave function does not change much in the large-r region, where it is "isolated" from the core electron. Thus, it is useful to have MQDT wave functions that emphasize the large-r symmetries for analyzing ICE spectra. Although autoionizing states, by their very nature, exhibit strong configuration mixing insofar as they are coupled to continuum configurations, the ICE studies have most often produced spectra showing doubly excited sequences with constant quantum defects and simply varying autoionization linewidths, even when many bound and continuum configurations (channels) could be involved.[8,9] A significant portion of this manuscript will be devoted to the analysis of ICE spectra for two reasons: (1) to show that the simple ICE results are consistent with an MQDT treatment, and that the positions and linewidths are those simple MQDT parameters referred to above; and (2) the ICE spectral analysis primarily involves an examination of the Rydberg electron's wave function, and thus is a prototype for any study of the properties of a two-electron Rydberg state.

Much of the mathematical treatment presented here is essentially similar to the MQDT works of Seaton;[1,10] the use of quantum defects and channel couplings is also very similar to the molecular work of Jungen and Dill[11] and of Giusti.[12] However, this work develops a geometrical interpretation of the MQDT equations and a vectorial

analysis which leads to the equivalent N-level formalism. We believe that these two aspects make approximations and conceptual solutions far easier. As an example, if one wishes to expand an analysis from N channels to $N+1$ channels (because a new perturbing configuration is identified), the formalism presented here allows an almost trivial extension which incorporates all the previous parameters, essentially unchanged. Such is often not the case when using the Fano formalism. Furthermore, this formulation easily allows multiphoton excitation extensions, which we have used to calculate four-wave-mixing line shapes[13] and two-photon shakeup dynamics.[14]

In the next section we will derive MQDT equations for a simple, model system—a spin-$\frac{1}{2}$ particle in a box. This illustrates the derivation technique and its accompanying mathematics in the simplest possible case. Section III extends the derivation to multielectron atoms, presents the geometrical picture of MQDT, and introduces the equivalent N-level system which serves as an intuitive guide for solving the MQDT equations. Section IV presents classes of solutions and approximate solutions, with a particular emphasis on the type of spectra resulting from photoabsorption from Rydberg states.

II. SPIN-$\frac{1}{2}$ PARTICLE IN A BOX

To illustrate the origin and form of the MQDT equations, we will begin by considering an MQDT formulation of the simple spin-$\frac{1}{2}$ particle in a square well with a magnetic spin coupling at one end. We will show how a doubly infinite series of states can be treated simply when viewed from a scattering formalism point of view. The MQDT solution will also illustrate how channel interactions affect the bound-state spectrum.

Consider the square well illustrated in Fig. 1. In the region $0<x<a$, there is a small magnetic field which can serve to mix spin states. If the magnetic field is in the z direction, then the spin up (called m_1 here) and spin down (m_2) are not mixed by the field and the problem is separable into two independent cases. To obtain the functional form of the wave function in the region $a<x<L$, consider the scattering of a spin-up plane wave $m_1\exp(-ikx)$, incident from the right-hand side of the well. Since probability must be conserved, all that can occur is a phase shift, so that the reflected wave is $m_1\exp[+i(kx+2\Delta)]$. By combining ingoing and outgoing plane waves, we can form standing waves of the form

$$\begin{aligned} m_1\sin(kx+\Delta_1)&=m_1\sin(kx)\cos\Delta_1+m_1\cos(kx)\sin\Delta_1\ ,\\ m_2\sin(kx+\Delta_2)&=m_2\sin(kx)\cos\Delta_2+m_2\cos(kx)\sin\Delta_2\ , \end{aligned} \tag{1}$$

where the m_i are the spin functions and the Δ_i depend on the magnetic field in the region $0<x<a$. Any wave function which satisfies the boundary condition at $x=a$ must be expressible as a linear combination of wave functions of the form of Eq. (1).

If the magnetic field B is not parallel to the z axis, then we must first pick the appropriate combination of spinors which are either parallel or antiparallel to the magnetic field

$$M_\alpha=\sum_i U_{i\alpha}m_i\ . \tag{2}$$

For example, if the magnetic field were along the x axis, the appropriate unitary transformation matrix is

$$\underline{U}=\frac{1}{\sqrt{2}}\begin{bmatrix}1 & 1\\ -1 & 1\end{bmatrix}\ . \tag{3}$$

With the new spinors M_α, we can form a basis set of wave functions analogous to those of Eq. (1) which match the boundary conditions at $x=a$:

$$\begin{aligned}\psi_\alpha=M_\alpha\sin(kx+\Delta_\alpha)=&\left[\sum_i U_{i\alpha}m_i\sin(kx)\right]\cos\Delta_\alpha\\ &+\left[\sum_i U_{i\alpha}m_i\cos(kx)\right]\sin\Delta\alpha\ .\end{aligned} \tag{4}$$

The boundary conditions at $x=L$ can be matched by inspection, and so we may also write down a basis set of wave functions which match the right-hand boundary condition

$$\begin{aligned}\phi_i=m_i\sin[k(x-L)]=&m_i\sin(kx)\cos(kL)\\ &-m_i\cos(kx)\sin(kL)\ .\end{aligned} \tag{5}$$

Now any valid wave function Ψ must match the left *and* right boundary conditions. Thus it must be expressible as a linear combination of the basis sets of Eqs. (4) and (5),

$$\Psi=\sum_i A_i\phi_i=\sum_\alpha B_\alpha\psi_\alpha\ . \tag{6}$$

If we now equate the coefficients of the spin-up (-down) times $\sin(kx)$ [$\cos(kx)$], we obtain four simultaneous equations:

$$\begin{aligned} A_1\cos(kL)&=U_{11}B_1\cos\Delta_1+U_{12}B_2\cos\Delta_2\ ,\\ -A_1\sin(kL)&=U_{11}B_1\sin\Delta_1+U_{12}B_2\sin\Delta_2\ ,\\ A_2\cos(kL)&=U_{21}B_1\cos\Delta_1+U_{22}B_2\cos\Delta_2\ ,\\ -A_2\sin(kL)&=U_{21}B_1\sin\Delta_1+U_{22}B_2\sin\Delta_2\ . \end{aligned} \tag{7}$$

These may be combined using complex exponentials to il-

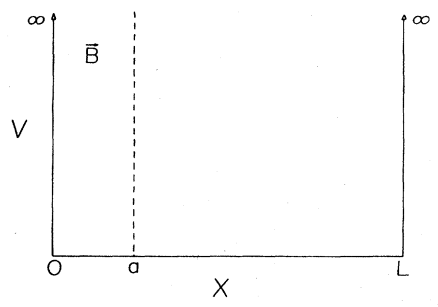

FIG. 1. Potential for a one-dimensional spin-$\frac{1}{2}$ particle in a box. The interaction between spin-up and spin-down states occurs in the region $0<x<a$, and is caused by the magnetic field **B**.

lustrate better the symmetry of the equations:

$$A_i e^{-ikL} = \sum_\alpha U_{i\alpha} B_\alpha e^{i\Delta_\alpha} , \tag{8a}$$

$$B_\alpha e^{i\Delta_\alpha} = \sum_i U_{i\alpha} A_i e^{-ikL} . \tag{8b}$$

Since the wave functions of Eqs. (4) and (5) are real, we can require A_i and B_α to be real, so that after multiplying Eq. (8a) by $\exp(ikL)$, we obtain

$$A_i = \sum_\alpha U_{i\alpha} \cos(\Delta_\alpha + kL) B_\alpha , \tag{9a}$$

$$0 = \sum_\alpha U_{i\alpha} \sin(\Delta_\alpha + kL) B_\alpha . \tag{9b}$$

In a similar fashion we can obtain an equivalent set of equations,

$$B_\alpha = \sum_i U_{i\alpha} \cos(\Delta_\alpha + kL) A_i , \tag{10a}$$

$$0 = \sum_i U_{i\alpha} \sin(\Delta_\alpha + kL) A_i . \tag{10b}$$

In order for either Eq. (9b) or (10b) to have a nontrivial solution, the coefficient matrix must have a zero eigenvalue, so that

$$\det | U_{i\alpha} \sin(\Delta_\alpha + kL) | = 0 . \tag{11}$$

In this simple case, since the right-hand boundary condition does not depend on m_i, we find that Eq. (11) reduces to

$$0 = \sin(\Delta_1 + kL) \sin(\Delta_2 + kL) , \tag{12}$$

which gives us the conditions on k for which valid solutions will exist.

If $B=0$ so that $\Delta_1 = \Delta_2 = 0$, we have the standard particle in a box and Eq. (12) is solved by

$$k_0 = N\pi/L , \tag{13a}$$

$$E_0 = N^2\pi^2/2L^2 , \tag{13b}$$

where atomic units ($\hbar = m = e = 1$) have been used. If a small, nonzero field is then applied, we would expect that $\Delta_1 = -\Delta_2 = \Delta$, and each eigenstate splits into two according to

$$k - k_0 = \pm\Delta/L , \tag{14a}$$

$$E - E_0 = \pm N\pi\Delta/L^2 . \tag{14b}$$

For this example, the phase shifts Δ_i will themselves depend on k or E when E is not large; however, we will ignore this complication. For the multielectron atom, the corresponding phase shifts will have only a weak dependence on energy. So, with the assumption that the Δ_i are energy independent, the spectra of this system is illustrated in Fig. 2. If the pair splitting is divided by the energy spacing between pairs, then we find that for large N, this ratio only depends on Δ. In the next section, we will see a similar effect for Rydberg states, where shifts from unperturbed values, divided by the spacing between unperturbed states, determine the fundamental physical interactions.

In this simple case, no information about $U_{i\alpha}$ can be obtained from the energy levels, since $U_{i\alpha}$ depends on the direction of B, not its magnitude. To obtain the $U_{i\alpha}$, we must know something about the wave functions for some of the eigenstates. This is also a general property of the MQDT analyses of atomic spectra. It is only possible to determine MQDT parameters completely when some information is known about wave functions—energy-level locations alone are not sufficient.

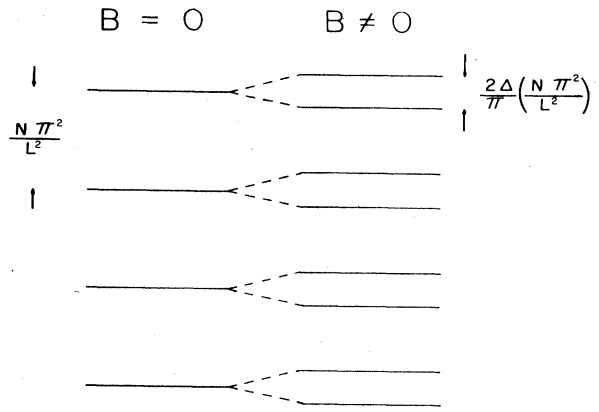

FIG. 2 High-N spectra for a one-dimensional spin-$\frac{1}{2}$ particle in the potential of Fig. 1.

III. MULTIELECTRON RYDBERG STATES

A highly excited state of a multielectron atom can usually be well approximated as a sum of a small number of product wave-function configurations. For each configuration a Rydberg electron is selected out, leaving the other electrons in a frozen ionic core. For different energy Rydberg states, the primary changes will be in the relative admixtures of different type configurations and in the Rydberg electron wave function itself. The different core configurations will be relatively insensitive to energy. MQDT is designed to address only those major changes, so for example, it accounts rather well for the changing mixture of $4dns, {}^1D_2$ and $5snd, {}^1D_2$ type configurations in strontium Rydberg states and for the changing Rydberg wave function. But changes in the $5s$ or $4d$ core wave functions are assumed to be negligible.

Under this approximation, the Schrödinger equation for the Rydberg electron at large r (where the potential is just Coulombic) is separable, and the solutions are products of spherical harmonics and Coulomb radial wave functions. In this case, the problem has effectively reduced to the one-dimensional problem of the previous section. The "wall" at $x = L$ has become the Coulomb potential $-Z/r$, which continues as $r \to \infty$. The spinor must be generalized to include not only the Rydberg electron's spin, but also its spherical harmonic and the appropriate core configuration. The magnetic field B is generalized to include all interactions between the Rydberg electron and the core—with the net effect that it still just causes mixings of the generalized spinors. We will next illustrate this correspondence in some detail, by way of developing

the MQDT equations for a multielectron atom.

A set of basis wave functions which matches the boundary conditions as $r \to \infty$ can be written

$$\phi_i = [s(W_i,r)\cos(\pi\nu_i) + c(W_i,r)\sin(\pi\nu_i)]\chi_i \ . \quad (15)$$

The s and c functions are Seaton's[10] regular and irregular solutions of the Coulomb radial equation for an electron of energy W_i [similar to $\sin(kx)$ and $\cos(kx)$ in Sec. II, and equivalent to the f and g functions of Fano[7]]. The parameter ν_i describes the relative admixture of regular and irregular solutions, and χ_i is a product of the angular part of the Rydberg electron's wave function, the core electrons' wave function, and the spinors for all electrons.

The wave functions ϕ_i are called collision channels, since they are a natural choice as $r \to \infty$. Examples of collision channels in strontium would be $5snd,{}^1D_2$; $5snd,{}^3D_2$; $4d_{5/2}ns$; $4d_{3/2}ns$. Different collision channels may be distinguished by their core state, their spin state, or the l of the Rydberg electron.

The energy of a collision channel is composed of two parts: W_i, the Rydberg electron's energy and I_i, the core-configuration energy (i.e., the ionization limit of the ϕ_i collision channel, Rydberg sequence). For $W_i < 0$, the s and c functions have exponentially growing and decaying parts as $r \to \infty$. The collision channel of Eq. (15) will only have exponentially decaying parts if ν_i is chosen so that

$$W_i = -\frac{1}{2\nu_i^2} \ . \quad (16)$$

In this case ν_i is commonly called the effective quantum number relative to the ith ionization limit, and the ith collision channel is called a closed channel. If two different collision channels, i and j, have the same ionization limit, then $\nu_i = \nu_j$ for all states of energy less than the ith ionization limit.

In some MQDT treatments, such as those of Lee and Lu[15] and Esherick,[16] the condition that $\nu_i = \nu_j$ (for two closed channels converging to the same limit) was introduced at the beginning to reduce the number of MQDT equations. In Esherick's work, for example, the two channels $5snd,{}^1D_2$ and $5snd,{}^3D_2$ were assigned the same parameter ν_i when both channels were closed. We will not apply this restriction at the outset since that would force a different behavior on closed channels than on open ones. Rather, we will *only* apply any energy conditions to the closed channels' ν_i *after* the equations are solved. In this way we will obtain the entire range of $\{\nu_i\}$ sets which match the boundary conditions near $r=0$, regardless of whether the collision channels are closed or not.

For bound states, this may seem an unnecessary complication. It allows the possibility of the $5snd,{}^1D_2$ and $5snd,{}^3D_2$ channels having different values of ν_i—which is impossible for bound states. However, for channels that are not closed, the ν_i parameters will generally *not* be equal. Thus, by not applying this condition early, we will show the general structure of *all* solutions.

If $W_i > 0$, then the s and c functions both oscillate as $r \to \infty$, with the s function 90° out of phase with the c function. Equation (15) then satisfies the boundary condition for any choice of ν_i as $r \to \infty$, since it is always finite. In this case $-\pi\nu_i$ is simply the phase shift relative to pure hydrogenic solutions. Channels for which $W_i > 0$ are called open channels, and the determination of ν_i arises entirely from matching the boundary conditions as $r \to 0$. As we will show below, a proper choice of channel composition and phase shifts $(-\pi\nu_i)$ will produce all zeros in the reaction matrix for the open channels.

To match the boundary conditions as $r \to 0$, we must, just as in the last section, construct a basis set valid in the region where r is small but the potential is simply $-Z/r$ (so that s and c functions are valid solutions). If the potential is just a Coulomb potential for all $r > r_c$, then a basis set which matches the boundary conditions at $r = r_c$ can be formed:

$$\psi_\alpha = \left[\sum_i U_{i\alpha}\chi_i s(W_i,r)\right]\cos(\pi\mu_\alpha) - \left[\sum_i U_{i\alpha}\chi_i c(W_i,r)\right]\sin(\pi\mu_\alpha) \ . \quad (17)$$

This basis set is essentially the same as that defined in Eq. (4) with the m_i spinor replaced by our generalized spinor χ_i, Δ_α is replaced by $-\pi\mu_\alpha$, $\sin(kx)$ is replaced by s, and $\cos(kx)$ is replaced by c. So again we can make the correlation that the linear combination of channels represented by $U_{i\alpha}$ is a normal mode of the scattering—one which has the same composition before and after a scattering event. Similarly, $-\pi\mu_\alpha$ is the scattering phase shift for the αth normal mode. The sum over i in Eq. (17) includes different spin states, Rydberg electron l states, and ion-core states. Consequently, the s and c functions cannot be factored out of the sum, as would be possible in Eq. (4), since they depend on the l of the Rydberg electron and on its energy W_i. For example, the Rydberg electron in a $5snd,{}^1D_2$ channel will have nearly 2 eV more energy than the Rydberg electron in a $4d_{3/2}ns$ channel, since the ion core has absorbed the additional energy. Only the total energy, $I_i + W_i$, is necessarily the same in the sum in Eq. (17). When $W_i > 0$ for all channels, the basis set of Eq. (17), called the close-coupled channels, are the natural, decoupled solutions of the multichannel problem.

In general, or at least where the spectrum shows resonances, $W_i < 0$ for some channels. Then the boundary conditions as $r \to \infty$ do play some role. The role of both boundary conditions can be taken into account, as in Sec. II, by requiring a valid solution Ψ, to be expressible as a linear combination of the basis channels of Eqs. (15) and (17) simultaneously,

$$\Psi = \sum_i A_i\phi_i = \sum_\alpha B_\alpha\psi_\alpha \ . \quad (18)$$

If the coefficients of $\chi_i s(W_i,r)$ and $\chi_i c(W_i,r)$ are equated, we again obtain

$$A_i e^{-i\pi\nu_i} = \sum_\alpha U_{i\alpha}B_\alpha e^{i\pi\mu_\alpha} \ , \quad (19a)$$

$$B_\alpha e^{i\pi\mu_\alpha} = \sum_i U_{i\alpha}A_i e^{-i\pi\nu_i} \ . \quad (19b)$$

The requirement that A_i and B_α be real, again reduces Eq. (19) to

$$A_i=\sum_\alpha U_{i\alpha}\cos[\pi(\nu_i+\mu_\alpha)]B_\alpha\ , \tag{20a}$$

$$0=\sum_\alpha U_{i\alpha}\sin[\pi(\nu_i+\mu_\alpha)]B_\alpha\ , \tag{20b}$$

or

$$B_\alpha=\sum_i U_{i\alpha}\cos[\pi(\nu_i+\mu_\alpha)]A_i\ , \tag{21a}$$

$$0=\sum_i U_{i\alpha}\sin[\pi(\nu_i+\mu_\alpha)]A_i\ . \tag{21b}$$

Equations (20) are those commonly used in the Fano MQDT formalism.[7] Equations (21) are an equivalent set. Either Eq. (20b) or (21b) requires for a nontrivial solution:

$$\det|\,U_{i\alpha}\sin[\pi(\nu_i+\mu_\alpha)]\,|=0\ . \tag{22}$$

Equation (22) is a restriction on the possible sets of values of ν_i which will match the boundary conditions as $r\to r_c$. As such, it describes an $(N-1)$-dimensional surface in the N-dimensional $(\nu_i)_{\mathrm{mod}\ 1}$ space.

The MQDT equations [(20) or (21)] can be used in either of two ways. If the parameters $U_{i\alpha}$ and μ_α are known (for example, if they are calculated *ab initio*), then Eq. (22) and the energy equation (16) can be used to determine all the bound states of a spectrum. Below, we will also show how the state composition, i.e., the A_i values, are also determined. On the other hand, if a spectrum is known, then some information can be obtained about the $U_{i\alpha}$ and μ_α parameters by using the energy equation (16) to determine what sets of ν_i are allowed. Since these sets must satisfy Eq. (22), restrictions can be put on $U_{i\alpha}$ and μ_α.

A. An alternate formulation

For an N-channel problem, Fano defines N^2 elements of the $U_{i\alpha}$ matrix and N μ_α phase shifts. However, since the $U_{i\alpha}$ matrix is an orthogonal matrix, it involves only $N(N-1)/2$ independent parameters to describe its N^2 elements. The redundancy involved in describing $N(N+1)/2$ total parameters with twice that number of elements introduces difficulties into fitting a spectrum, or into characterizing the significance of individual elements. These difficulties are illustrated by the standard way an orthogonal matrix is constructed from a product of $N(N-1)/2$ rotation matrices. The effects are cumulative, so that if the first rotation mixes channels 1 and 2, then the second rotation will mix the rotated channel 2 and channel 3. Stated another way, if a different ordering of rotation matrices were used, the same $U_{i\alpha}$ would require a different set of rotation angles. Thus, the rotation angles alone (without knowing their ordering) are not a unique representation of $U_{i\alpha}$.

All of these difficulties can be avoided by constructing a symmetrical matrix with only $N(N+1)/2$ total elements from the $U_{i\alpha}$ matrix and the μ_α phase shifts. Accordingly, we can rewrite the MQDT equation (21b) in a fashion that eliminates the $U_{i\alpha}$ and μ_α elements in favor of a symmetric matrix which has eigenvalues equal to $\tan(\pi\mu_\alpha)$ and eigenvectors given by the columns of $U_{i\alpha}$. Rewriting (21b), we find

$$\cos(\pi\mu_\alpha)\left\{\sum_i\left[U_{i\alpha}\tan(\pi\nu_i)+\tan(\pi\mu_\alpha)U_{i\alpha}\right]\cos(\pi\nu_i)A_i\right\}=0 \tag{23}$$

or

$$\{\tan(\pi\mu)\underline{\mathbf{U}}^T+\underline{\mathbf{U}}^T\tan(\pi\nu)\}\mathbf{a}=\mathbf{0} \tag{24}$$

where $\tan(\pi\mu)$ and $\tan(\pi\nu)$ are diagonal matrices and $a_i=\cos(\pi\nu_i)A_i$. Multiplying Eq. (24) by $\underline{\mathbf{U}}$ and since $\underline{\mathbf{U}}^{-1}=\underline{\mathbf{U}}^T$, we obtain

$$[\underline{\mathbf{R}}+\tan(\pi\nu)]a=\mathbf{0}\ , \tag{25}$$

$$\underline{\mathbf{R}}=\underline{\mathbf{U}}\tan(\pi\mu)\underline{\mathbf{U}}^T\ . \tag{26}$$

Equation (26) is essentially the form that Seaton used to determine the bound-state spectra in his formalism of MQDT.[10] The matrix $\underline{\mathbf{R}}$ has the desired simplification that it is real and symmetric, thus having only $N(N+1)/2$ elements as required. Furthermore, it has an apparent similarity to a conventional effective Hamiltonian matrix.

B. The geometrical interpretation

To evaluate Eq. (22), it is useful to define a cofactor matrix $C_{i\alpha}$, the elements of which are cofactors of the coefficient matrix of Eqs. (20b) or (21b)

$$C_{i\alpha}=\mathrm{Cofactor}\{U_{i\alpha}\sin[\pi(\nu_i+\mu_\alpha)]\}\ . \tag{27}$$

The determinant of Eq. (22) may now be evaluated by expanding along a row or column,

$$\begin{aligned}0&=\det|\,U_{i\alpha}\sin[\pi(\nu_i+\mu_\alpha)]\,|\\&=\sum_i U_{i\alpha}\sin[\pi(\nu_i+\mu_\alpha)]C_{i\alpha}\\&=\sum_\alpha U_{i\alpha}\sin[\pi(\nu_i+\mu_\alpha)]C_{i\alpha}\ .\end{aligned} \tag{28}$$

By comparing Eq. (28) with Eqs. (20b) and (21b), we can identify that B_α must be proportional to any row of $C_{i\alpha}$ and A_i must be proportional to any column. Thus,

$$C_{i\alpha}=GA_iB_\alpha\ , \tag{29}$$

where G is some proportionality constant.

We can now complete the geometrical interpretation of the MQDT formulation by evaluating the gradient of the surface defined by Eq. (22),

$$\begin{aligned}&\frac{\partial}{\partial\nu_j}\det|\,U_{i\alpha}\sin[\pi(\nu_i+\mu_\alpha)]\,|\\&\quad=\sum_\alpha\left[\frac{\partial}{\partial\nu_j}U_{j\alpha}\sin[\pi(\nu_j+\mu_\alpha)]\right]C_{j\alpha}\\&\quad=\pi GA_j^2\ .\end{aligned} \tag{30}$$

In Eq. (30) we expanded the determinant along the jth row. $C_{j\alpha}$ does not depend on ν_j by construction, so the differentiation is simple. The sum over α was then done by substituting for $C_{j\alpha}$ from Eq. (29) and using Eq. (20a) to eliminate the sum over α. Equation (30) demonstrates that the normal to the $(N-1)$-dimensional surface of Eq. (28) has projections along the ν_i axes which are proportional to A_i^2.

This geometrical interpretation can best be illustrated by using a three-channel example. Figure 3 is a surface which solves Eq. (22) for some choice of $U_{i\alpha}$ and μ_α. A particular eigenstate Ψ from Eq. (18) is represented by a point on that surface. The normal to the surface at that point has components proportional to A_1^2, A_2^2, and A_3^2, respectively. If, for example, the point lies anywhere in the large flat region near $\nu_1=0$, the state has mostly ϕ_1 character. Similarly, if it lies on the flat region near $\nu_2=0$, it has mostly ϕ_2 character. The regions where the wave functions are composed of nearly equal amounts of two or more channels are those with a sizable amount of curvature.

The shape of the surface in Fig. 3 is in fact quite typical insofar as the existence of the large flat regions. That these large flat regions occur near $\nu_i=0$ is a quirk of the particular choice of MQDT parameters for Fig. 3. But in most of the spectra which have been analyzed by MQDT so far, the flat regions exist. It is not always possible to identify these regions in the bound-state spectra, since the energy restriction on ν_i of Eq. (16) may preclude *bound* states from lying on a particular flat region. These regions are made more obvious as the energy restrictions are reduced in the autoionizing region. In general, the bound-state spectra will not show many aspects of the multidimensional surface, since each energy level will only place a point on the surface and these points will only sparsely cover the available area. However, once the first ionization threshold is crossed, the solutions form a line on the surface. And for each subsequent threshold that is crossed, an additional line of solutions is added. Consequently, the autoionizing region can provide much greater coverage of the surface of Eq. (22) than the bound spectra can.

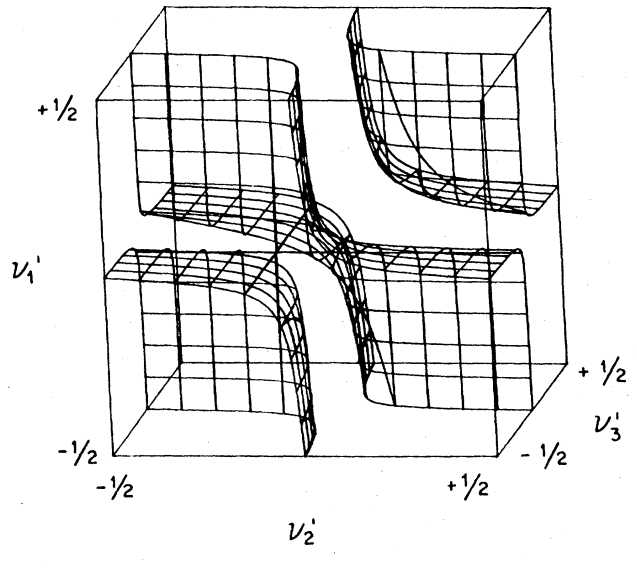

FIG. 3. Surface representing the allowable choices of $\{\nu_1',\nu_2',\nu_3'\}$ to solve a typical MQDT equation. The state composition at any given point is determined by the projection of the normal to the surface along the ν_i axes. So points in the large flat region near $\nu_1'=0$ correspond to states with mostly ϕ_1 character, points near $\nu_2'=0$ correspond to states with mostly ϕ_2 character, and points on the curved regions correspond to states with highly mixed character.

This suggests that a natural subdivision of MQDT parameters into two distinct sets should be possible. One set would be composed of δ_i values, such that if $\delta_i+\nu_i$ is an integer, the wave function would have primarily ϕ_i character. The δ_i values can easily be obtained from an MQDT surface since $-\delta_i$ corresponds to the intercept where a plane tangent to the flat region cuts across the ν_i axis. These δ_i values are, of course, the single-channel quantum defects. The other set of MQDT parameters, which will be independent from the single-channel quantum defects δ_i would represent only interactions between channels, i.e., channel mixings. These parameters would only affect the curvature of the surface of Eq. (22) and would be small (so long as flat regions exist, the curvature cannot be too large).

To separate out the single-channel quantum defects δ_i, we can translate the ν_i parameters by defining

$$\nu_i'=\nu_i+\delta_i\ , \tag{31}$$

$$a_i'=A_i\cos(\pi\nu_i')\ . \tag{32}$$

Then, Eq. (25) can be rewritten as

$$\{\underline{\mathbf{R}}'+\tan(\pi\nu')\}\mathbf{a}'=\mathbf{0}\ , \tag{33}$$

where $\underline{\mathbf{R}}'$ is the symmetric matrix:

$$\begin{aligned}\underline{\mathbf{R}}'&=[\cos(\pi\delta)+\mathbf{R}\sin(\pi\delta)]^{-1}[\mathbf{R}\cos(\pi\delta)-\sin(\pi\delta)]\\&=\cos(\pi\delta)/\sin(\pi\delta)-[\sin(\pi\delta)\mathbf{R}\sin(\pi\delta)\\&\quad+\sin(\pi\delta)\cos(\pi\delta]^{-1}\ ,\end{aligned} \tag{34}$$

with $\cos(\pi\delta)$ and $\sin(\pi\delta)$ representing diagonal matrices. Seaton[10] has also described this transformation of $\underline{\mathbf{R}}$.

The transformations of Eqs. (32) and (34) represent changing the radial wave-function basis set of s and c functions to new linear combinations as done by Eissner *et al.*[17] These new functions, instead of being regular or irregular near the origin, represent solutions with phase shifts of $\pi\delta_i$ and $\pi(\delta_i+\frac{1}{2})$ relative to hydrogen. This new basis set is more natural since the δ_i parameters can allow for nonhydrogenic, spherical perturbations to the Rydberg electron. Thus, the δ_i can account for the typically large quantum defects that exist for low l states, even in the absence of multiconfigurational effects (e.g., $\delta_s=1.35$ in sodium).

The only effect to remain in $\underline{\mathbf{R}}'$, if the large spherical effects are absorbed in the δ_i, is just the channel mixings. Unless these mixings are so severe that the approximation of an average spherical Rydberg potential is invalid, the elements of $\underline{\mathbf{R}}'$ should be smaller than the typical differ-

ences in δ_i between channels. A severe channel mixing is not to be confused with the existence of a severely perturbed state. Even small perturbations can cause a drastic change in state composition, if the perturbing state is close by in energy. For example, the $5s7s,{}^1S_0$ state of strontium is nearly equally mixed with the $5p^2,{}^1S_0$ state. A large value of an element of $\underline{\mathbf{R}}'$, on the other hand, would mean that *all* $5sns$ states would be heavily perturbed. An example of this behavior can be provided by the $5snd,{}^{1,3}D_2$ states of strontium. If one chose the *jj*-coupled $5snd_{3/2}$ and $5snd_{5/2}$ channels as the basis set, then one would find that the channel mixing between them would be large and its result would be to recouple *all* states back into singlet and triplet states. If the channel composition and the single-channel quantum defects δ_i are appropriately chosen, however, the elements of $\underline{\mathbf{R}}'$ should be small.

We have found it convenient to require the diagonal elements of $\underline{\mathbf{R}}'$ to be zero, when fitting spectra. The N δ_i and $N(N-1)/2$ off-diagonal elements of $\underline{\mathbf{R}}'$ are then varied independently to obtain a fit. On the other hand, *ab initio* calculations can sometimes be more easily done by allowing small, nonzero diagonal elements of $\underline{\mathbf{R}}'$. For example, the exchange interaction can mix the $4d_{3/2}ns$ and $4d_{5/2}ns$ channels of strontium, but it will also produce different δ_i for the two channels. It might be easier in this case to use one value of δ for both channels while allowing diagonal $\underline{\mathbf{R}}'$ elements, since the diagonal and off-diagonal elements are simply related. In any case, Eq. (34) allows for an easy transformation so that the δ_i or diagonal $\underline{\mathbf{R}}'$ elements may be chosen in whatever fashion is convenient for the problem.

C. The N-level system

It is somewhat easier to understand the form of the solutions to Eq. (33) by defining an equivalent *N-level* system with an effective Hamiltonian

$$\underline{\mathbf{R}}'+\tan(\pi\nu'),$$

and a total pseudoenergy E:

$$[\underline{\mathbf{R}}+\tan(\pi\nu')]\mathbf{a}'=E\mathbf{a}' , \tag{35}$$

where a' is a vector describing the composition of an eigenstate constructed from the original N basis states. The matrix $\tan(\pi\nu')$ then describes an unperturbed, diagonal Hamiltonian, and $\underline{\mathbf{R}}'$ is the perturbation which causes mixing of the N states into eigenstates $\mathbf{a}'$. The eigenstates $\mathbf{a}'$ will also describe an MQDT solution whenever its pseudoenergy E is zero. Thus, the equivalent N-level system allows us to express quantum defects and channel mixings as effective Hamiltonians and reduces the boundary conditions to an equivalent energy restriction.

Consider the use of the equivalent N-level system as illustrated for two channels in Fig. 4. Here we have chosen $\delta_1=\delta_2=0$ for simplicity, so that $\underline{\mathbf{R}}=\underline{\mathbf{R}}'$ and has only the one element R'_{12}, and $\nu_i=\nu'_i$. If $R'_{12}=0$, then there are two unperturbed Rydberg series (i.e., series with constant quantum defects, zero in this case), converging to two different ionization limits $I_1<I_2$. For a small, nonzero R'_{12}, the state having $\nu'_1=22$, is shifted up by an amount

$$\Delta E_1=\frac{\nu'_1-22}{\nu'^3_1}\approx\frac{\tan(\pi\nu'_1)}{\pi\nu'^3_1} \tag{36}$$

since ν'_1-22 is sufficiently small that $\tan(\pi\nu'_1)$ can be expanded. Similarly, the same state is shifted from the $\nu'_2=15$ state by

$$\Delta E_2=\frac{\nu'_2-15}{\nu'^3_2}\approx\frac{\tan(\pi\nu'_2)}{\pi\nu'^3_2} . \tag{37}$$

Now if $\tan(\pi\nu'_1)<\tan(\pi\nu'_2)\ll 1$, then the equivalent two-level system may be solved by second-order perturbation theory

$$E=\tan(\pi\nu'_1)+\frac{(R'_{12})^2}{\tan(\pi\nu'_1)-\tan(\pi\nu'_2)}=0 , \tag{38}$$

$$\tan(\pi\nu'_1)\approx\frac{(R'_{12})^2}{\tan(\pi\nu'_2)} , \tag{39}$$

$$\Delta E_1=\frac{(R'_{12})^2}{\pi^2\nu'^3_1\nu'^3_2}\frac{1}{\Delta E_2} , \tag{40}$$

where we have applied the MQDT restriction that $E=0$, and used Eqs. (36) and (37) to introduce real energy shifts. But Eq. (40) is exactly what we would have expected if we had associated an interaction, V_{12} between the unperturbed states $\nu'_1=22$ and $\nu'_2=15$ such that

$$V_{12}=-\frac{R'_{12}}{\pi(\nu_1\nu_2)^{1.5}} . \tag{41}$$

This means that $-R'_{12}/\pi$ is the interaction between the unperturbed channels ϕ_1 and ϕ_2 defined in Eq. (15). The scaling with ν_1 and ν_2 is to be expected, since the channels defined in Eq. (15) have an energy-independent amplitude near the core and are thus normalized so that for bound channels

$$\int\phi_i^2 r^2\,dr=\nu_i^3 . \tag{42}$$

Thus, the $\underline{\mathbf{R}}'$ matrix coupling N channels can be calculated as easily as can a perturbing Hamiltonian between N states using Eq. (41).

It will usually be possible to find a state near one of the unperturbed states (since there are large flat regions in the MQDT surface), so that the analysis leading to Eqs. (42) and (43) will be valid; however, not all states will have $\tan(\pi\nu'_i)\ll 1$ for all i. It is useful to consider a state where $\tan(\pi\nu'_i)\to\infty$ for one i to see the significance of the tangent function. Consider the system of Fig. 4 again; however, this time note the state $\nu'_1=23$. For a nonzero R'_{12} this state will remain unshifted using the second-order perturbation analysis of Eq. (39), since $\tan(\pi\nu'_2)$ is very large ($\nu'_2=15.5$).

The equivalent N-level system consists of two states far separated by energy, so that second-order shifts are negligible. But now consider the state composition, by evaluating a'_2 from first-order perturbation theory and then relating it to A_2 by Eq. (32)

$$A_2=\frac{1}{\cos(\pi\nu'_2)}\frac{R'_{12}}{\tan(\pi\nu'_2)}\approx R'_{12} . \tag{43}$$

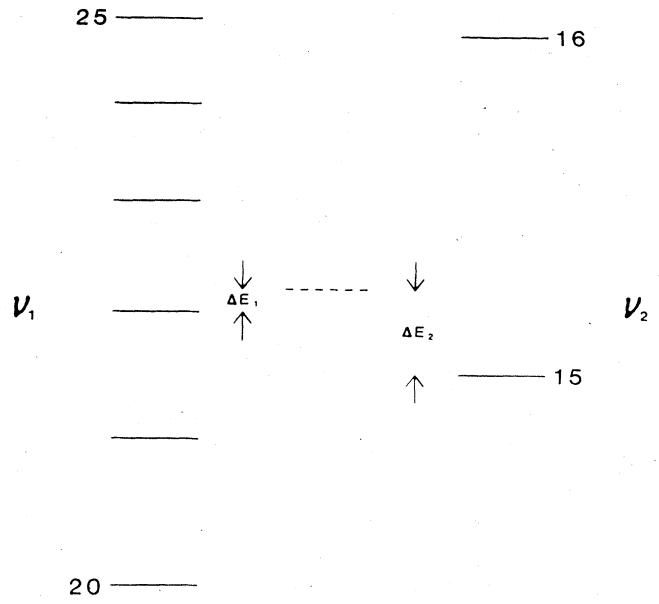

FIG. 4. Two unperturbed Rydberg series (solid lines) which converge to two different ionization limits, $I_1 < I_2$. The left and right scales show effective quantum numbers relative to the I_1 and I_2 limits. The dashed line designated the position of an eigenstate when the channel interaction is introduced. The energy shifts ΔE_1 and ΔE_2 represent the energy shift of the eigenstate from the nearest unperturbed state of channels 1 and 2, respectively.

Thus, we see that the unperturbed state $\nu_1' = 23$ suffers no energy shift from the interaction R_{12}', but does have ϕ_2 character mixed into it. Figure 4 illustrates the origin of this: the unperturbed state $\nu_1' = 23$ is shifted up due to its interaction with the unperturbed state $\nu_2' = 15$, but it is simultaneously shifted down by its interaction with the unperturbed state $\nu_2' = 16$. The energy shifts cancel, although the admixture of the two different ϕ_2 wave functions cannot cancel. Thus, the use of the tangent function becomes a shorthand way to sum over an infinite number of states (including the continuum) and replace it with one effective state in our equivalent N-level system. In his formulation of one perturber interacting with an "almost-continuum" of high Rydberg states, Fano illustrates how the tangent function can be obtained directly from such a sum.[18]

IV. SOLUTIONS TO THE N-LEVEL SYSTEM

A. Bound states

The eigenvector equation (33) will always have N-independent solutions; however, only those for which the eigenvalue $E=0$ will be solutions of the MQDT equations. Nevertheless, if the offset parameters δ_i of Eq. (31) are approximately chosen, the $\underline{\mathbf{R}}'$ matrix will have small elements so that approximate solutions will give an excellent picture as to what is the wave function composition and what energies are allowed.

Once Eq. (33) is solved, with the restriction that $E=0$, the eigenvector $\mathbf{a}'$ can be used to obtain a properly normalized wave function

$$\Psi = C\left[\sum_i A_i \phi_i\right] = C \sum_i [1+\tan^2(\pi\nu_1')]^{1/2} a_i' \phi_i \ , \tag{44a}$$

$$C = \left[\sum_i A_i^2 \nu_i^3\right]^{-1/2} = \left[\sum_i [1+\tan^2(\pi\nu_i')](a_i')^2 \nu_i^3\right]^{-1/2} , \tag{44b}$$

where the normalization constant C has been evaluated by normalizing the wave function to unity, using Eq. (42).

Note that in Eq. (44a), A_i^2 describes the relative admixture of collision channels ϕ_i. If the ϕ_i channels had been normalized to unity themselves, the relative admixture would have been $\nu_i^3 A_i^2$. A simple classical analog explains these two sets of coefficients. The values A_i^2 describe the percentage of orbits in which the Rydberg electron stays in any given configuration. Thus, if $A_1^2 = \frac{1}{3}$, and $A_2^2 = \frac{2}{3}$, the Rydberg electron would average one orbit in configuration 1 for every two orbits in configuration 2. But different orbits have different periods. Since ν_i^3 is proportional to the classical period, the quantity $A_i^2 \nu_i^3$ is proportional to the average time spent in configuration i. The A_i coefficients best describe the Rydberg electron—ion-core collision, but a real measurement will usually average over some time rather than a specified number of orbits. Thus, both normalization procedures are useful.

B. Autoionizing states

If there are n_c open or continuum channels, then there will be at least n_c solutions to Eq. (35) which simultaneously satisfy the $E=0$ condition. This is because the n_c values of $\tan(\pi\nu_i')$ for the open channels are no longer related to the energy directly, but can be chosen at will to solve Eq. (35). To solve for those vectors and $\tan(\pi\nu_i')$ values, it is useful to divide the $\underline{\mathbf{R}}' + \tan(\pi\nu')$ matrix into four quadrants which connect open channels to open channels, open channels to bound channels, bound channels to bound channels, and bound channels to open channels as shown below (where "b" represents bound and "c" represents continuum or open):

$$\underline{\mathbf{R}}' \tan(\pi\nu') = \begin{bmatrix} [\underline{\mathbf{R}}' + \tan(\pi\nu')]_{bb} & \underline{\mathbf{R}}'_{bc} \\ \underline{\mathbf{R}}'_{cb} & [\underline{\mathbf{R}}' + \tan(\pi\nu')]_{cc} \end{bmatrix} . \tag{45}$$

Then, following the procedure outlined by Seaton,[10] we obtain n_c solutions by requiring that $\tan(\pi\nu_i') = \varepsilon_j$ for each continuum channel i where j is an index between 1 and n_c enumerating the independent solutions. This allows us to solve Eq. (35) simply, reducing it to an n_c-dimensional eigenvalue problem:

$$\{\underline{\mathbf{R}}'_{cb}[\underline{\mathbf{R}}' + \tan(\pi\nu')]_{bb}^{-1} \underline{\mathbf{R}}'_{bc} - \underline{\mathbf{R}}'_{cc}\} \mathbf{a}_c' = \varepsilon_j \mathbf{a}_c' \ , \tag{46a}$$

$$\mathbf{a}_b' = -[\underline{\mathbf{R}}' + \tan(\pi\nu')]_{bb}^{-1} \underline{\mathbf{R}}'_{bc} \mathbf{a}_c' \ . \tag{46b}$$

Equations (46) have n_c different continuum solutions, each of which is normalized according to

$$\sum_{\{n_c\}} A_i^2=[(\varepsilon_j)^2+1]\sum (a_c')^2=1 , \tag{47}$$

since only one orbit is allowed in a continuum configuration.

In Eq. (46a) the matrix coefficient is the same as the reaction matrix of Seaton's formulation;[10] and the ε_j values are thus the eigenvalues of the reaction matrix. Lee and Lu[15] define a phase shift τ in the autoionizing region, whose tangent is the value $-\varepsilon_j$. Lee and Lu[15] also define a T matrix composed of the n_c sets of continuum wavefunction coefficients A_{cj}. We have avoided these additional definitions to stress the continuity of MQDT as one passes from a bound to a continuum energy region.

The solutions outlined above will not be complete if there exists a vector $\mathbf{a}'$ such that

$$\mathbf{a}_c'=\mathbf{0} , \tag{48a}$$

$$\{\underline{\mathbf{R}}'+\tan(\pi\nu')\}_{bb}\mathbf{a}_b'=\mathbf{0} , \tag{48b}$$

$$\underline{\mathbf{R}}'_{cb}\mathbf{a}_b'=\mathbf{0} . \tag{48c}$$

Under these circumstances, the vector $\mathbf{a}'$ will represent a completely bound state, degenerate with, but uncoupled to, the continua.

In a similar fashion, one can often construct combinations of the n_c continuum channels such that they no longer couple to any one (or any one set) of the bound channels. Thus, if $n_b<n_c$ (where n_b is the number of bound channels), one can construct n_c-n_b such continuum channels that do not couple to the bound channels at all. Since only $\tan(\pi\nu')_{bb}$ depends on energy, the uncoupled continua channels can *only* add a constant background to any spectrum. All of the features of the spectrum can be constructed from an equivalent set of only $2n_b$ channels. Fano demonstrated this same type of simplification for the case of one isolated level interacting with two continua.[18]

C. Approximate solutions

Since the MQDT equations have been replaced by an energy restriction on an equivalent N-level system, it becomes possible to apply all of the well-known approximation techniques to the MQDT problem. Specifically, any interaction between channels 1 and 2 will cause them to repel each other. In the absence of other channels the eigenvalues of the perturbed state if $R'_{11}=R'_{22}=0$ will be

$$E=\tfrac{1}{2}([\tan(\pi\nu_2')+\tan(\pi\nu_1')] \pm\{[\tan(\pi\nu_2')-\tan(\pi\nu_1')]^2+4R'^2_{12}\}^{1/2}) . \tag{49}$$

Consequently, solutions with a zero eigenvalue can only occur when $\tan(\pi\nu_1')$ and $\tan(\pi\nu_2')$ are either both positive or both negative. Geometrically, this shows up (in N dimensions) as the requirement that the surface defined by Eq. (22) must have a normal whose projections along the N axes all have the same sign. Without this restriction, Eq. (30) could not always be valid. For our two-channel example, two cases stand out, corresponding to $|\tan(\pi\nu_2')-\tan(\pi\nu_1')|$ being much less or much greater than $|R'_{12}|$.

If $|\tan(\pi\nu_2')-\tan(\pi\nu_1')\ll|R'_{12}|$, the solution can be obtained from degenerate perturbation theory, requiring

$$\tan(\pi\nu_2')\approx\tan(\pi\nu_1')\approx R'_{12} . \tag{50}$$

The wave functions are obtained from setting $a'_1=\pm a'_2$, and since $\tan(\pi\nu_2')=\tan(\pi\nu_1')$,

$$A_2=\pm A_1 . \tag{51}$$

That is, one obtains symmetric or antisymmetric combinations of channels 1 and 2. Figure (5a) schematically shows this solution by illustrating the eigenvalues of the $\tan(\pi\nu')$ matrix and the new eigenvalues of the $\tan(\pi\nu')+\underline{\mathbf{R}}'$ matrix (where we have picked $R'_{11}=R'_{22}=0$). For the correct choice of $\tan(\pi\nu_1')$ and $\tan(\pi\nu_2')$ one of the new eigenvalues is zero.

If $|\tan(\pi\nu_2')-\tan(\pi\nu_1')|\gg|R'_{12}|$, the simple perturbation analysis applied in the earlier section holds and a solution is obtained for $\tan(\pi\nu_1')$ satisfying Eq. (39) and a wave function such that

$$A_2=\left[\frac{1+\tan^2(\pi\nu_2')}{1+\tan^2(\pi\nu_1')}\right]^{1/2}\frac{R'_{12}}{\tan(\pi\nu_2')-\tan(\pi\nu_1')}A_1 . \tag{52}$$

Figure (5b) schematically shows this case, again illustrating eigenvalues before and after the perturbation.

For more than two channels, the above approximations are readily expanded, using degenerate perturbation theory when $|\tan(\pi\nu_i')-\tan(\pi\nu_j')|<|R'_{ij}|$ and regular perturbation theory otherwise. Since first-order perturbation theory is additive, the only new complication that can occur is when degenerate perturbation theory must be used for several channels. In that case the solutions are approximately the eigenvectors and eigenvalues of the matrix $\underline{\mathbf{R}}'$ restricted to only those channels lying in the degenerate band. Since $\underline{\mathbf{R}}'$ is independent of energy, these degeneracies can only introduce a small number of complications. Far more often, the solution will be readily

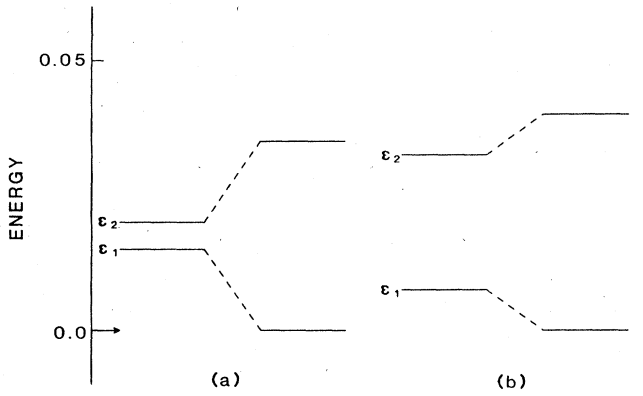

FIG. 5. Pseudoenergies are shown before and after including the R'_{12} interaction which repels the states; ϵ_1 and ϵ_2 represent the respective values of $\tan(\pi\nu_1')$ and $\tan(\pi\nu_2')$. In (a) $|\tan(\pi\nu_2')-\tan(\pi\nu_1')|\ll R'_{12}$ so that the solution ($\epsilon=0$) has has nearly equal admixtures of ϕ_1 and ϕ_2. In (b) $|\tan(\pi\nu_2')-\tan(\pi\nu_1')|\gg R'_{12}$, so that the solution has mostly ϕ_1 character. For both cases $R'_{12}=0.02$; the arrow designates $\epsilon=0$, the condition under which the MQDT equations are solved.

handled by first-order perturbation theory, where at most a twofold degeneracy must be removed.

D. Photoionization spectra for highly excited states

In an increasing number of experiments, the isolated core excitation (ICE) technique has been used to study autoionizing states. It simply illustrates the essentials of using MQDT to predict or to model spectra, particularly using the formalism developed here. We will briefly describe the ICE technique and then describe expected spectra and their analysis in some detail.

The wave function of a two-electron-like atom (e.g., alkaline-earth atoms) in a bound, Rydberg state usually consists of mostly one configuration, having an unexcited "core" electron and a high-n "Rydberg" electron. Although many channels may be required to describe the state fully, the normalized wave function will be dominated by the one configuration. This occurs because, as described above, the normalized wave function represents a time-averaged distribution and the electron's orbit is far longer in a Rydberg orbit. Thus, to model the absorption spectra from a Rydberg state, it is usually sufficient to consider only the one, dominant configuration as the initial wave function. For example, the absorption spectra of an excited state of barium that has both $6sns$ and $5d\,7d$ configurations will be dominated by the $6sns$ absorption characteristics over a large wavelength range.[19]

Furthermore, optical absorptions from the two-electron Rydberg state will be dominated by the core ionic transitions. Direct photoionization of the Rydberg electron is always a weak process since the Rydberg electron would be ejected so far above threshold. The core electron, on the other hand, still responds strongly to light near the ionic core resonances. It is in this sense that absorptions from bound Rydberg states correspond to isolated core excitations. Under these circumstances, it has been shown that the dipole transition matrix element from an initial state $|g\nu^g l\rangle$ (where g represents the ion-core ground state and the Rydberg state is represented by its effective quantum number ν^g and angular momentum l) to a final autoionizing state $|e\nu^e l'\rangle$ is given by

$$\mu=\langle g\nu^g l\,|\mu|\,e\nu^e l'\rangle = \mu_{ge}\delta_{ll'}\frac{\sin[\pi(\nu^g-\nu^e)]}{\pi(\nu^g-\nu^e)}\frac{(4\nu^g\nu^e)^{1/2}}{\nu^g+\nu^e}\,, \tag{53}$$

where μ_{ge} is the transition moment for the isolated ion from state g to state e, and $\delta_{ll'}$ is the Kronecker delta, and ν^e is the effective quantum number relative to the excited-ion ionization limit. This transition moment corresponds to the transition moment for the ion (completely isolated) times an overlap factor which projects the initial Rydberg wave function onto the final Rydberg wave function, as in a sudden approximation.[19,20]

But, as we have seen in the previous sections, the wave functions in the autoionizing region are not well represented by single configurations (here the time-averaging argument would vastly favor the continuum channel), so the transition moment must be modified to account for the relative amount of the $|e\nu^e l'\rangle$ configuration in the true final wave function.

Now, if $|e\nu^e l'\rangle$ corresponds to a closed collision channel i, then expression (53) must only be modified by $(\nu^e)^{3/2}A_i$. The expression then simplifies to

$$\mu=(\nu^g)^{-3/2}\mu_{ge}\frac{\sin[\pi(\nu^g-\nu^e)]}{\pi(W_g-W_e)}A_i\,, \tag{54}$$

where W_g and W_e are the binding energies of the Rydberg electron in the initial and final configurations, respectively.

For a given absorption spectra, since ν^g is fixed when the excited, bound Ryberg state is prepared, only two factors from Eq. (54) can produce features in the absorption profile. The first factor, $\sin\pi(\nu^g-\nu^e)/(W_g-W_e)$ produces a broad variation, requiring zeroes between each different member of a Rydberg series and suppressing all transitions where $|\nu^g-\nu^e|$ is large. The widths of features produced solely by this factor would be nearly 50% of the spacing between features. Far more often, the widths and locations of features are determined by the second factor A_i so that the ICE technique often provides a simple, direct measurement of the autoionizing wave function in terms of the collision-channel coefficients. The variation of channel coefficients will easily determine the MQDT parameters.

This can be illustrated with a two-channel example, in which we assume a transition moment only to the bound channel 1, so that the effect of the open channel 2 can be easily seen. If we further choose $R'_{11}=R'_{22}=0$ [by choosing appropriate δ_i shifts according to Eq. (34)], then Eqs. (46) and (47) can be solved,

$$\tan(\pi\nu'_2)=\frac{(R'_{12})^2}{\tan(\pi\nu'_1)}\,, \tag{55a}$$

$$A_1=-R'_{12}\left[\frac{1+\tan^2(\pi\nu'_1)}{(R'_{12})^4+\tan^2(\pi\nu'_1)}\right]^{1/2}\,. \tag{55b}$$

Thus A_1^2 almost has the functional form of a Lorentzian (see Fig. 6). For small values of R'_{12}, this leads to a full

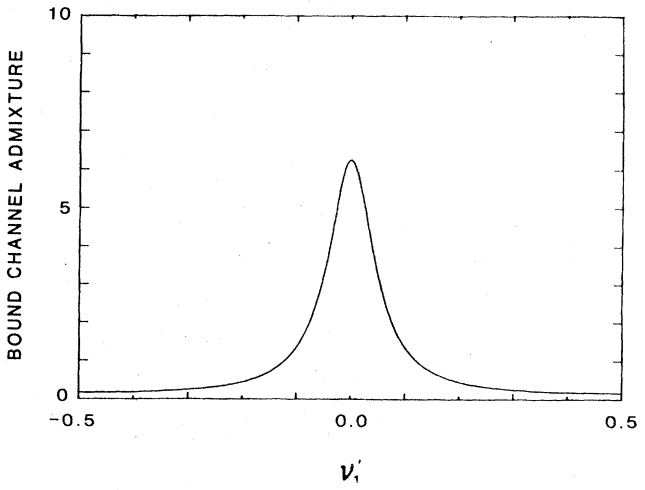

FIG. 6. A_1^2 vs ν'_1 for a two-channel case, with channel 2 open, $R'_{11}=R'_{22}=0$; $R'_{12}=0.4$. A_1^2 reaches a maximum value at 6.25 and a minimum at 0.16.

width at half maximum, Γ, in the spectrum of

$$\Gamma=\frac{2(R'_{12})^2}{\pi\nu_1^3}\ , \tag{56}$$

where we have used Eq. (36) to relate an interval in $\tan(\pi\nu'_1)$ to an energy interval. A_1^2 reaches its maximum value of $(R'_{12})^{-2}$ when $\tan(\pi\nu'_1)=0$, that is when $\delta_1+\nu_1$ is an integer. No information can be obtained from such a spectrum regarding δ_2, since the continuum wave function has played no role except for normalization through Eq. (47). Nevertheless, two of the three MQDT parameters have been easily determined this way.

If more than two channels are involved, the additional channels will cause different effects depending on whether they are open or closed. If the channels are open, the problem is no more difficult, so we will consider that case first. One can begin by choosing a new continuum basis set composed of linear combinations of the original basis set. For the correct combination, the $\underline{\mathbf{R}}'_{cc}$ matrix will be diagonalized. This will, of course, create a new R'_{1c} vector. After this basis reconstruction, the open channels will have a new definition and the ν_i will refer to the new basis. As an example, if originally channel 2 was $4d_{3/2}ns$ and channel 3 was $4d_{5/2}ns$ for strontium, then if both channels were open, a better choice (to diagonalize $\underline{\mathbf{R}}_{cc}$) might be

$$\begin{aligned}|\,4dns,{}^1D_2\,\rangle&=(\tfrac{3}{5})^{1/2}\,|\,4d_{5/2}ns\,\rangle=(\tfrac{2}{5})^{1/2}\,|\,4d_{3/2}ns\,\rangle\ ,\\ |\,4dns,{}^3D_2\,\rangle&=-(\tfrac{2}{5})^{1/2}\,|\,4d_{5/2}ns\,\rangle+(\tfrac{3}{5})^{1/2}\,|\,4d_{3/2}ns\,\rangle\ .\end{aligned} \tag{57}$$

In this case ν_2 would now refer to the combination coefficient as defined in Eq. (15) for a pure ${}^1D_2$ state, and ν_3 would be for a pure ${}^3D_2$ state.

Once we have diagonalized $\underline{\mathbf{R}}'_{cc}$, we can shift the MQDT parameters according to Eq. (31) to obtain $\underline{\mathbf{R}}'_{cc}=0$. A final rotation of the basis set would result in the bound channel-1 coupling to one new continuum channel. This rotation, however, would maintain the length of the R'_{1c} vector, so we can immediately use Eq. (55) to write down the spectrum

$$A_1=-\left[\left[\frac{\pi\nu_1^3\Gamma}{2}\right]\frac{1+\tan^2(\pi\nu'_1)}{\left[\frac{\pi\nu_1^3\Gamma}{2}\right]^2+\tan^2(\pi\nu'_1)}\right]^{1/2}\ , \tag{58a}$$

$$\Gamma=\frac{2}{\pi\nu_1^3}\sum_{\{n_c\}}(R'_{1j})^2\ . \tag{58b}$$

Again, the spectrum easily yields δ_1 and the sum of the squared interaction strengths to each continuum channel. Without a branching ratio measurement, no information can be obtained about the individual R'_{1c}. Similarly, no information is available about the original $\underline{\mathbf{R}}_{cc}$.

If the additional channels are bound, they can either introduce new structure or just cause a variation in the observed line positions and widths. Consider only one additional bound channel, $i=3$. If the ν_i parameters are shifted according to Eq. (31) until $R'_{ii}=0$ for all three channels, then Eq. (46) and (47) can be easily solved to obtain A_1^2

$$A_1^2=\frac{[1+\tan^2(\pi\nu'_1)][\tan(\pi\nu'_3)R'_{12}-R'_{13}R'_{23}]^2}{[\tan(\pi\nu'_1)\tan(\pi\nu'_3)-(R'_{13})^2]^2+[\tan(\pi\nu'_3)(R'_{12})^2+\tan(\pi\nu'_1)(R'_{23})^2-2R'_{12}R'_{13}R'_{23}]^2}\ . \tag{59}$$

If $\nu_3\ll\nu_1$, as would be the case when channel 3 converges to a higher ionization limit than channel 1 (channel 2 is open), then ν_3 will be nearly constant as ν_1 varies over an integer cycle. The additional channel 3 will then only change the observed spectral positions and widths rather than introduce new structure. To illustrate this, we can rewrite Eq. (59) in terms of a shift s_1 and a width b_1 that are functions of the slowly varying $\tan(\pi\nu'_3)$,

$$A_1^2=\frac{[1+\tan^2(\pi\nu'_1)]b_1}{[\tan(\pi\nu'_1)-s_1]^2+b_1^2}\ , \tag{60a}$$

$$s_1=\frac{\tan(\pi\nu'_3)[(R'_{13})^2-(R'_{12})^2(R'_{23})^2]+2R'_{12}R'_{13}(R'_{23})^3}{\tan^2(\pi\nu'_3)+(R'_{23})^4}\ , \tag{60b}$$

$$b_1=\frac{[R'_{12}\tan(\pi\nu'_3)-R'_{13}R'_{23}]^2}{\tan^2(\pi\nu'_3)+(R'_{23})^4}\ . \tag{60c}$$

The width b_1 varies over a considerable range as a function of $\tan(\pi\nu'_3)$,

$$(b_1)_{\min}=0\quad\text{for}\ \tan(\pi\nu'_3)=\frac{R'_{13}R'_{23}}{R'_{12}}\ , \tag{61a}$$

$$(b_1)_{\max}=(R'_{12})^2+(R'_{13}/R'_{23})^2 \quad\text{for}\ \tan(\pi\nu'_3)=\frac{-R'_{12}(R'_{23})^3}{R'_{13}}\ . \tag{61b}$$

For very large $\tan(\pi\nu'_3)$, the width reduces to the two-channel case of Eq. (55b). For smaller $\tan(\pi\nu'_3)$, Eq. (60c) shows that the width (and thus the autoionization rate) of channel 1 is composed of two interfering parts: (1) direct autoionization represented by R'_{12} and (2) indirect autoionization through channel 3 represented by $R'_{12}R'_{23}/\tan(\pi\nu'_3)$. These two autoionization routes interfere since they lead to the same final product—channel 2. The interference can produce a minimum width of zero, as in Eq. (61a). This would correspond to the truly bound, doubly excited state in the continuum referred to in Eq. (48).

At the other extreme of the interference, Eq. (61b) shows that b_1 can become quite large. If $(R'_{23})^2=1$, then according to Eq. (55b) with "3" substituted for "1," the isolated 2–3 system would result in no structure and channel 3 would look just like a continuum channel. In this case Eq. (61b) would give a maximum width that exactly corresponds to the one-bound—two-continua case of Eq. (58b). For different values of R'^2_{23}, the maximum rate

is either decreased or enhanced as the 1—3 interaction is either spread out over a larger range, or compressed to a sharper channel resonance.

These effects are illustrated in Fig. 7, which shows the reduced linewidth $\nu_1^3\Gamma$ of $6p_{1/2}ns$ states for $n=18$—30. This reduced linewidth is the width measured in ν_1 units, and is thus proportional to b_1 for small values. Near the vicinity of the $6p_{3/2}10d$ perturber, the linewidths show a resonant, asymmetric increase, ranging from a minimum value of 0.05 to a maximum of nearly 0.3. The width does not decrease to a true zero since there are actually many continuum channels involved, and each will have its effect cancelled at a slightly different value of ν_1. Figure 7 also shows a fit to the values of the linewidth of these resonances using a numerical solution of a four-channel MQDT.[21] Although the zero has been removed, the general properties of the asymmetric resonance are the same in a four-channel or a three-channel MQDT.

The shift s_1, also representing an interference, can also vary over a wide range

$$(s_1)_{\min}=0 \quad \text{for } \tan(\pi\nu_3')\to\pm\infty$$

$$\text{or } \tan(\pi\nu_3')=\frac{2R'_{12}R'_{13}(R'_{23})^3}{(R'_{12})^2(R'_{23})^2-(R'_{13})^2}\ , \tag{62a}$$

$$(s_1)_{\max}=\mp\tfrac{1}{2}(R'_{12}\pm R'_{13}/R'_{23})^2$$

$$\text{for } \tan(\pi\nu_3')=\pm(R'_{23})^2\frac{(R'_{12}R'_{23}\mp R'_{13})}{(R'_{12}R'_{23}\pm R'_{13})}\ . \tag{62b}$$

The maximum shift also depends on both the 1—3 interaction and the 3—2 continuum coupling. If $R'_{23}=0$, as for a bound channel, then the shift can result in effective quantum number ν_1 changes as large as $\pm\frac{1}{2}$. Usually, in the autoionizing region, however, the effective quantum numbers (and thus the apparent "quantum defects") will vary much less dramatically. Figure 8 shows the slight variation in effective quantum numbers for the same $6p_{1/2}ns$ states which show the dramatic width variation in Fig. 7. For these autoionizing states a "Lu-Fano" plot is deceptive since the perturbing $6p_{3/2}10d$ state is spread over a large region along the ν_1 axis and thus averages out the large shifts that would be expected had the perturber been bound. The width variation is a much better guide to the channel interactions in this case. Figure 8 also shows the calculated values of the apparent quantum defects, using the same parameters as used to fit the widths.[21]

If the additional channel 3 converges to a lower limit than channel 1, then $\nu_3\gg\nu_1$ and, as the energy is varied ν_3 will pass through several cycles while ν_1 is nearly constant. In this case new structure will appear in the ICE spectrum, and it is useful to rewrite Eq. (59) in terms of the rapidly changing variable $\tan(\pi\nu_3')$,

$$A_1^2=(R'_{12})^2\frac{1+\tan^2(\pi\nu_1')}{(R'_{12})^4+\tan^2(\pi\nu_1')}\frac{[\tan(\pi\nu_3')-s_3-q_3b_3]^2}{[\tan(\pi\nu_3')-s_3]^2+b_3^2}\ , \tag{63a}$$

$$s_3=\frac{\tan(\pi\nu_1')[(R'_{13})^2-(R'_{12})^2(R'_{23})^2]+2R'_{13}R'_{23}(R'_{12})^3}{\tan^2(\pi\nu_1')+(R'_{12})^4}\ , \tag{63b}$$

$$b_3=\frac{[\tan(\pi\nu_1')R'_{23}-R'_{13}R'_{12}]^2}{\tan^2(\pi\nu_1')+(R'_{12})^4}\ , \tag{63c}$$

$$q_3=\frac{\tan(\pi\nu_1')R'_{13}+(R'_{12})^3R'_{23}}{R'_{12}[\tan(\pi\nu_1')R'_{23}-R'_{12}R'_{13}]}\ . \tag{63d}$$

The first factor in Eq. (63a) represents the basic envelope of a two-channel line shape as in Eq. (55b). The second factor is a rapid modulation, each cycle of ν_3 representing a basic Beutler-Fano line shape of width b_3, shift s_3, and "q" value q_3. The width and shift are the same as would be observed by exciting to the $i=3$ channel directly (i.e., measuring A_3^2), although the asymmetry is absent in such a direct measurement ($q_3\to\infty$). The envelope function effectively restricts $\tan(\pi\nu_1')$ to a range of $\pm(R'_{12})^2$, within

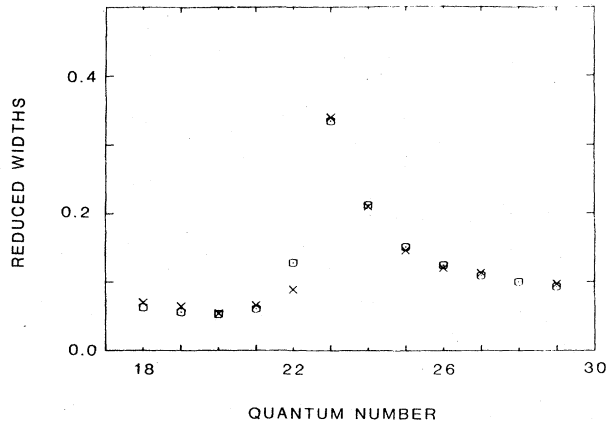

FIG. 7. Reduced widths ($\nu_1^3\Gamma$) of some $6P_{1/2}ns$ states of barium in the vicinity of the $6P_{3/2}10d$ perturber from as measured ($\times$) and as fit ($\square$) by a four-channel MQDT analysis (Ref. 21).

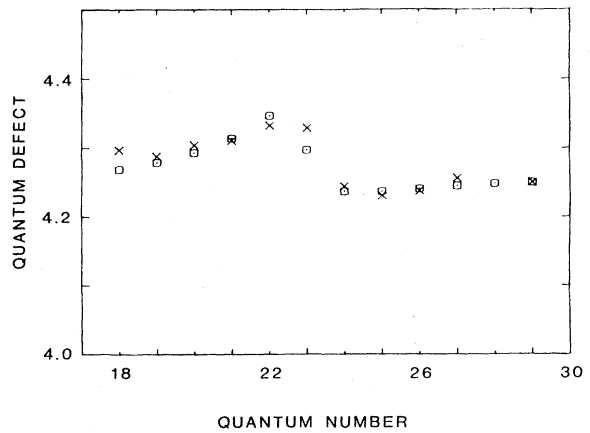

FIG. 8. Quantum defects of some $6P_{1/2}ns$ states as measured ($\times$) and as fit ($\square$) using the same MQDT analysis used in Fig. 7 (Ref. 21).

which the denominator of Eq. (63d) does not vary much. Over this range, q_3 may be approximated for small R'_{ij}

$$q_3 \approx -\frac{\tan(\pi\nu'_1)}{(R'_{12})^2} - \frac{R'_{23}R'_{12}}{R'_{13}} . \tag{64}$$

In Fig. 9, the ICE spectrum corresponding to $6s\,12s,{}^1S_0 \rightarrow 6p_{3/2}12s,J=1$ is shown. Through this energy range the state is perturbed by many $6p_{1/2}ns$ and $6p_{1/2}nd$ states. Near the center of the profile minima ($q_3=0$) are located near the resonances; whereas, in the wings maxima ($|q_3| \gg 1$) are near the perturbing resonances. The $6p_{1/2}ns$ resonances occur almost exactly midway between the $6P_{1/2}nd$ resonances, and can be clearly seen as additional peaks in the long-wavelength end of the spectrum. A six-channel MQDT fit is also shown for comparison.[21] Six channels were required since, as shown above, a general fit requires $n_c=n_b$ ($=3$ in this case). Without the full six channels, either the $6p_{1/2}ns$ resonances, or the background could not be fit. However, the essential features of Eq. (63a) remain.

In the wings of the spectrum, if we use the large $\tan(\pi\nu'_1)$ limits of Eqs. (63), we obtain a simple expression for the area under a feature

$$[(A_1)^2_{\max}]b_3 \approx R'^2_{13} . \tag{65}$$

This expression is consistent with a general expression derived using the perturbation theory technique used to obtain Eq. (43):

$$[(A_1)^2_{\max}]b_j = (R'_{1j})^2 . \tag{66}$$

Thus, the area under the features in the wings give the branching ratio for autoionization when those higher channels are open. In the case of Fig. 9, the spectra predicts that $6p_{3/2}ns$ states for $n>12$ will autoionize producing nearly three times as many $Ba^+(6p_{1/2})$ ions plus d-wave electrons as s-wave electrons.

The spectrum of Fig. 9 does not show true zeroes between the peaks as predicted by Eq. (63a). This is because there are more than one continua involved, so that again an interference effect can only lead to a partial cancellation. However, the perturbative analysis of the structure in the wings is still valid as long as the satellite peaks are clearly distinct, i.e., in the regions where the interference effects are due only to the two bound channels, $i=1$, and 3.

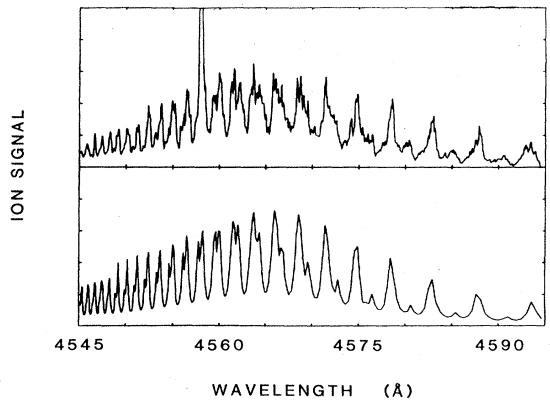

FIG. 9. ICE spectrum for the $6s\,12s,{}^1S_0 \rightarrow 6P_{3/2}12s,J=1$ transition in barium. The structure results from mixing with the $6P_{1/2}ns$ and $6P_{1/2}nd$ channels. The upper curve is the measurement, the lower curve is a fit that uses a six-channel MQDT analysis (Ref. 21). The large feature at 4557 Å is a wavelength marker.

V. CONCLUSION

In this work we have presented a simple derivation of the MQDT equations in order to emphasize the physical origin of their form. In a similar vein, we have suggested an alternative set of MQDT parameters which emphasize the physical interactions in a multichannel problem. Specifically, there are two groups of parameters: one set of quantum defects that represents the effects on the Rydberg electron of the average, spherical potential due to the core, and a second set of interchannel couplings that represents the mixing of different Rydberg l or S series due to anisotropies within the core. In addition to being physically intuitive, these parameters should be calculable by methods as simple as those used for calculating the characteristics of alkali atoms.

We have also presented a geometrical interpretation of the MQDT equations which allows one to deduce quickly and intuitively the eigenstate composition for any valid combination of effective quantum numbers. Similarly, in order to simplify the determination of what combination of effective quantum numbers are valid, we have introduced the equivalent N-level system (to replace N channels) which can be constructed from our MQDT parameters. The eigenstates of this system can be solved in standard fashions, and if a solution is found that has a pseudoenergy of zero, then this immediately identifies a solution of the original MQDT problem. Thus, we have replaced the boundary conditions of MQDT with an equivalent pseudoenergy condition in our N-level system. In many cases, this provides an easy technique for solving the MQDT equations.

To illustrate the use of the equivalent N-level system, we have treated the problem of photoionization of Rydberg states through autoionizing resonances. Using the ICE model, we have presented simple formulas that represent all of the various types of spectra to be expected. These spectra range from the simple autoionizing resonance (two-channel case) to complex line shapes showing many interferences; however, they are all easily treated with a small number of parameters.

Recent experiments that have observed autoionizing Rydberg states[8,9,14,19,21] have found that usually those states have nearly constant quantum defects, even in complex atoms, like barium. The analysis presented here has shown that since autoionizing states are not restricted to having a single-energy eigenvalue (as are bound states), their spectrum presents a broader picture of the solutions to the MQDT problem. Thus, the simplicity of the autoionizing states' spectra suggested a simplicity in MQDT. Our alternative MQDT parameters and our equivalent N-level formulation confirm that suggestion.

ACKNOWLEDGMENTS

We wish to thank U. Fano, T. F. Gallagher, R. R. Freeman, R. Shakeshaft, and P. Zoller for many useful discussions and comments. We particularly wish to thank L. Van Woerkom for a careful reading and discussion of the manuscript. This work was supported by the National Science Foundation under Grant No. PHY-80-01666. One of us (W.E.C.) wishes to acknowledge the support of the Alfred P. Sloan Foundation.

---

*Present address: National Bureau of Standards, Gaithersburg, MD 20899.

[1]M. J. Seaton, Proc. Phys. Soc. London **88**, 801 (1966).
[2]K. T. Lu and U. Fano, Phys. Rev. A **2**, 81 (1970).
[3]J. A. Armstrong, P. Esherick, and J. J. Wynne, Phys. Rev. A **15**, 180 (1977).
[4]M. Aymar and O. Robaux, J. Phys. B **12**, 531 (1979).
[5]R. Beigang and D. Schmidt, Phys. Scr. **27**, 172 (1983); H. Rinneberg and J. Neukammer, Phys. Rev. A **27**, 1779 (1983).
[6]C. M. Brown, S. G. Tilford, and M. L. Ginter, J. Opt. Soc. Am. **67**, 584 (1977).
[7]U. Fano, Phys. Rev. A **2**, 353 (1970).
[8]W. E. Cooke, T. F. Gallagher, S. A. Edelstein, and R. M. Hill, Phys. Rev. Lett. **41**, 178 (1978); S. A. Bhatti and W. E. Cooke, Phys. Rev. A **28**, 756 (1983).
[9]T. F. Gallagher, W. E. Cooke, and K. A. Safinya, in *Laser Spectroscopy IV,* edited by H. Walther and K. W. Rothe (Springer, New York, 1979), p. 273.
[10]M. J. Seaton, Rep. Prog. Phys. **46**, 167 (1983).
[11]C. Jungen and D. Dill, J. Chem. Phys. **73**, 1 (1980).
[12]A. Giusti, J. Phys. B **13**, 3867 (1980); A. Giust-Suzor and U. Fano, J. Phys. B **17**, 215 (1984).
[13]C. L. Cromer, Ph.D. thesis, University of Southern California, 1983.
[14]R. M. Jopson, R. R. Freeman, W. E. Cooke, and J. Bokor, Phys. Rev. Lett. **51**, 1640 (1983).
[15]C. M. Lee and K. T. Lu, Phys. Rev. A **8**, 1241 (1973).
[16]P. Esherick, Phys. Rev. A **15**, 1920 (1977).
[17]W. Eissner, H. Nussbaumer, H. E. Sarah, and M. J. Seaton, J. Phys. B **2**, 341 (1969).
[18]U. Fano, Phys. Rev. **124**, 1866 (1961).
[19]S. A. Bhatti, C. L. Cromer, and W. E. Cooke, Phys. Rev. A **24**, 161 (1981).
[20]J. Dubau, Ph.D. thesis, University of London, 1973.
[21]S. A. Bhatti, Ph.D. thesis, University of Southern California, 1983.